

Quarterly Report for
January - March 1999
Stanford Geothermal Program
DE-FG07-95ID13370

Table of Contents

1. MEASUREMENTS OF STEAM-WATER RELATIVE PERMEABILITY	1
1.1 INTRODUCTION	1
1.2 EXPERIMENTAL DESIGN	1
1.3 RESULTS	3
2. AN EXPERIMENTAL INVESTIGATION OF BOILING HEAT CONVECTION WITH RADIAL FLOW IN A FRACTURE	5
2.1 INTRODUCTION	5
2.2 DIFFERENCES IN EXPERIMENTAL PREPARATION	6
2.3 FUTURE WORK	7
3. INFERRING ENDPOINT SATURATION FROM BOILING EXPERIMENTS AND FIELD MEASUREMENTS	9
3.1 INTRODUCTION	9
3.2 INFERRING ENDPOINT SATURATION FROM BOILING EXPERIMENTS	10
3.3 INFERRING ENDPOINT SATURATION FROM FIELD MEASUREMENTS	15
4. STEAM-WATER CAPILLARY PRESSURE	18
4.1 INTRODUCTION	18
4.2 THEORY	18
4.3 EXPERIMENTS	21
4.4 RESULTS	22
4.5 CONCLUSIONS	23
4.6 FUTURE WORK	23
5. SLIP EFFECT IN STEAM FLOW	24
5.1 SUMMARY	24
5.2 INTRODUCTION	24
5.3 THEORY	26

5.4 EXPERIMENTS	28
5.5 EXPERIMENTAL RESULTS	29
5.6 DISCUSSION	32
5.7 CONCLUSTIONS	32
5.8 FUTURE WORK	33
6. REFERENCES	34

1. MEASUREMENTS OF STEAM-WATER RELATIVE PERMEABILITY

This project is being conducted by Research Assistant Glenn Mahiya and Professor Roland Horne. The aim is to measure relative permeability relations for steam and water flowing simultaneously in rocks.

1.1 INTRODUCTION

Steam-water relative permeability curves have been determined experimentally by Ambusso (1995) and Satik (1997) in the past under the Stanford Geothermal Program. An important concern, though, is that the repeatability of experimental results has not been established. Improvements in the experimental setup have been implemented, and we further these efforts with the installation of guard heaters to eliminate heat losses during the experiment. In the quarterly report for July–September 1998, we described in detail the flexible heaters that will be used for the experiment. These custom-made sheet heaters, each an array of independently controllable strip heaters, will compensate for whatever heat losses occur along the core and impose an adiabatic condition on the experiment. Eliminating the heat losses reduces the possible sources of errors, minimizes the time to reach equilibrium conditions, and allows for a larger two-phase zone over which saturations can be measured via the X-ray CT scanner.

In this report, we focus on the data acquisition and control system that we have developed to operate the flexible heaters.

1.2 EXPERIMENTAL DESIGN

The general experimental setup has been discussed in the last quarterly report and can be visualized by referring to Figure 1.1. Note that the Kapton-insulated heaters are wrapped around the coreholder. In between the heaters and the coreholder, heat flux sensors are positioned along the core for measuring (net) heat loss. Each heat flux sensor is connected to a panel that interfaces with the National Instruments data acquisition hardware. Currently, we have three data acquisition modules installed. One SCXI-1100 module processes data from the pressure transducers, while an identical module reads temperature from thermocouple devices and heat fluxes from the sensors. The third module is the SCXI-1163R, a 32-channel, optically isolated, solid state relay that we are using to control the guard heaters. We use the software LabView to gather, process and display data, as well as control devices such as the heaters.

Figure 1.2 illustrates the setup that minimizes heat losses. Note that since heat loss varies with distance from the inlet of the core, the heat replenishment will likewise vary accordingly to attain zero net heat flux everywhere. Aside from spatial variation, heat loss also changes with time especially in the early part of the experiment when equilibrium has not been reached. Since the SCXI-1163R controls a device by switching it on or off, there is no direct way of providing variable power to the heater. It is not feasible to obtain a constant output from the heater that is different from the maximum it can deliver given

since the voltage and current are fixed when the SCXI-1163R is used. Thus, a target level of heat output is achieved by essentially switching the heater on and off (digital proportional control). The on-time and off-time are determined by the measurements made by the heat flux sensors. The LabView "virtual instrument," a graphical subroutine, that controls the flexible heaters is shown in Figure 1.3.

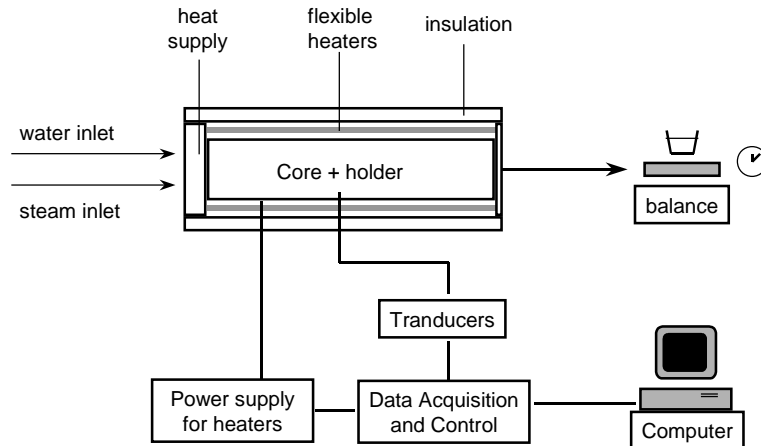


Figure 1.1: Schematic diagram of relative permeability experiment.

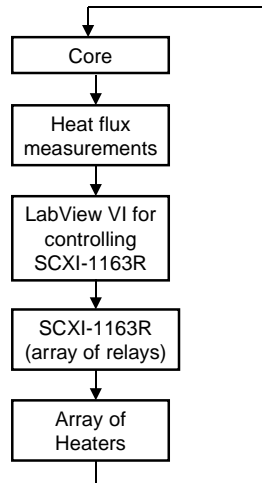


Figure 1.2: Control flow for flexible heaters.

A pulsing scheme shown in Figure 1.4 allows us to oscillate about the target heat flux with a small range of tolerable deviation set by the upper and lower limits. The heat flux measured serves as input to the sub-vi and is tested if it falls within the allowable range. If the value is within the range, the state of the heater (i.e., on or off) is not changed. Otherwise, an "on" signal will be sent if the heat flux falls below the lower limit, and an "off" signal is sent if the value goes beyond the upper limit. Since the heater has a finite characteristic response time (i.e., the time it requires to reach the maximum power) provides some advantage in that we do not always have to achieve the full power of the heater especially if the heat needed is well below the maximum deliverable output.

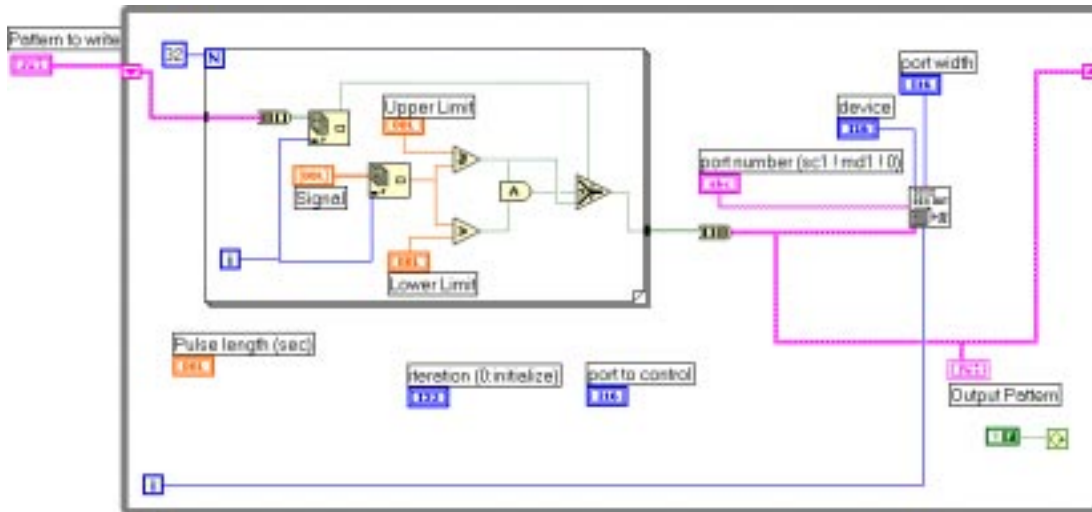


Figure 1.3: LabView virtual instrument for heater control.

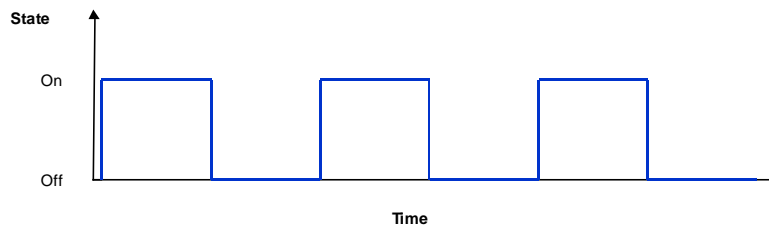


Figure 1.4: Pulsing scheme for controlling the guard heaters.

The advantage of using LabView is that results are displayed graphically in real time. This allows us to detect any abnormalities in the course of the experiment and correct them as necessary. From the continuous plot of heat flux sensor readings, it will be easy to see whether or not the flexible heaters are providing the appropriate amount of heat compensation.

1.3 RESULTS

In a series of preliminary experiments, a set of relative permeability curves have been measured (Figure 1.5) using the new apparatus. The results appear consistent with the recent results of Satik (1998) in that they show a curvilinear behavior not unlike the Corey curves. This is distinct from the linear "X curve" type of behavior measured in the earlier study by Ambusso, et al. (1996). The values of steam relative permeability greater than one have been explained as the effects of gas slippage (Klinkenberg effect), as described in Section 5 of this report).

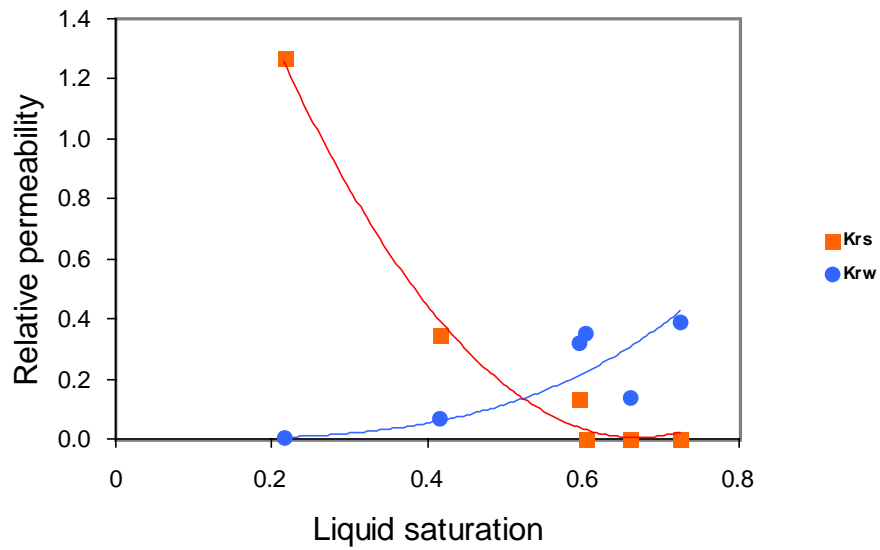


Figure 1.5: Steam-water relative permeability curves measured in February 1999.

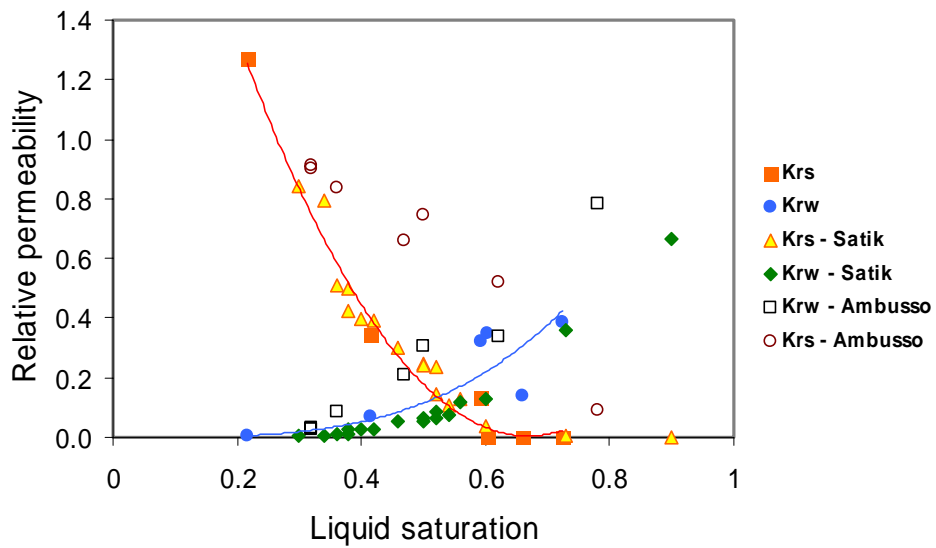


Figure 1.6: Steam-water relative permeability measurements compared to earlier studies.

2. AN EXPERIMENTAL INVESTIGATION OF BOILING HEAT CONVECTION WITH RADIAL FLOW IN A FRACTURE

This project is being conducted by Research Assistant Robb Barnitt and Professor Roland Horne. The goal is to investigate and compare the heat flux and temperature gradients that develop during boiling with liquid injection into a simulated rock fracture in a geothermal reservoir. Ultimately, this project intends to develop a boiling convection coefficient for use in calculating heat transfer with boiling in fractured geothermal rock. Improved understanding and modeling of heat transfer in a fracture will ultimately lead to better strategies for injection into fractured geothermal reservoirs.

2.1 INTRODUCTION

The experimental work conducted early this quarter included the experiment described in the October–December 1998 quarterly report, and presented at the Twenty-Fourth Stanford Workshop on Geothermal Reservoir Engineering on January 26, 1999. This recent experiment sought to investigate and compare the heat flux and temperature gradients that develop during boiling with liquid injection into a radial fracture, and examine the differences in behavior dependant upon the nature of the fracture boundary matrix. These experiments were designed to quantify the heat flux associated with liquid water flashing to steam in a fracture, and to investigate the degree of coupling between the heat flux and the vapor fraction flowing in the fracture. The experiment built upon graduate work conducted by Bob DuTeaux, who investigated these phenomena using samples of Geysers core (graywacke). The recent experiment conducted this January utilized highly porous sandstone, and non-porous aluminum. The experimental apparatus used during the Geysers core experiments was again used with the sandstone and aluminum.

A comparison of experimental data indicates that while heat transfer on nonporous surfaces is strongly coupled to the flow regime and vapor fraction, the heat flux to porous rock surfaces with boiling appears to be much less sensitive to the quantity of vapor flowing in the fracture. The thermodynamics of vaporization in porous media model the ΔT_c required for boiling, and the heat flux is influenced by matrix permeability as well as porosity.

One conclusion that can be drawn is that boiling in a fracture is not strictly a surface phenomenon even in very low porosity and low permeability rock, but that the rock porosity and permeability play important roles in either reducing or enhancing the coupling between the heat flux and the liquid/vapor ratio of the flow in the fracture.

Review of the experimental procedures and rock preparation employed in the original experiment using graywacke indicate that some enhancements may improve the quality of experimental data, and provide a better correlation with the recent sandstone and aluminum experiment.

2.2 DIFFERENCES IN EXPERIMENTAL PREPARATION

The apparatus illustrated in Figure 2.1 was utilized both in the original experiments using graywacke, and the more recent round of experiments using sandstone and aluminum. However, the preparation of rock samples and experimental procedures differed slightly.

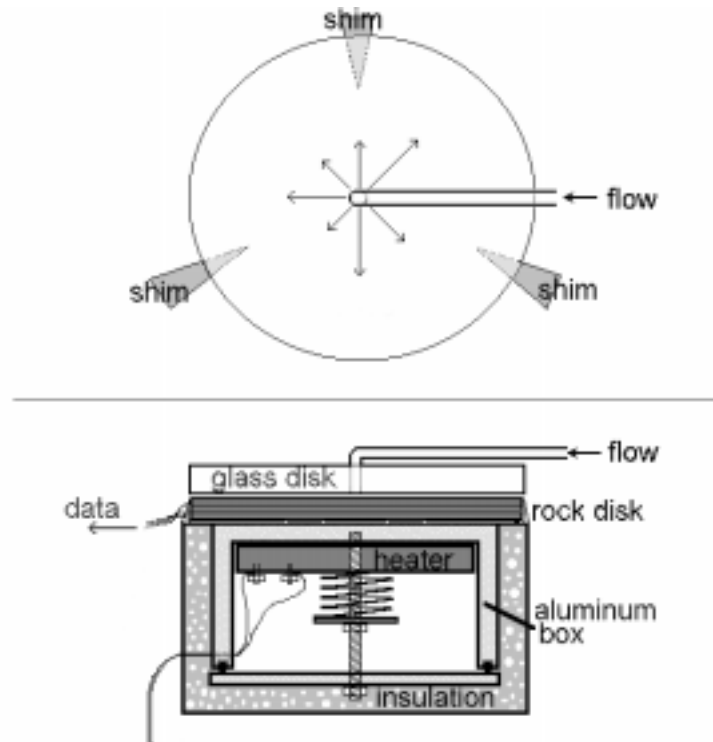


Figure 2.1: Heat flux-Temperature gradient measurement experimental apparatus.

In the original experiment using graywacke, three thin Geysers rock disks were prepared with a surface grinder to achieve flat well-mated surfaces. Thermocouples were placed on the aluminum heater box, and at each interface between rock disks. The outer edge of the rock was sealed with epoxy and silicone to prohibit radial flow within the rock and to restrain radial heat conduction. The thermocouples were located on the interfaces between disks radially 1.5 centimeters from the center, separated from one another by an angle of 120 degrees. Shallow grooves were cut in the rock surfaces for the placement of thermocouples. The top surface of the heater box was engraved to have thermocouples and heat flux sensor was placed on that surface at the base of the rock. Each of the rock disks, from the bottom to the top surface of the rock are, respectively, 3.10 mm, 4.19 mm, and 3.58 mm thick, and a set of three thermocouples were placed at each junction.

In the recent experiment using sandstone and aluminum, the aluminum disk and sandstone samples had small holes drilled at four different levels within the disk for a close tolerance fit with thermocouples. Again, the thermocouples were placed 1.5 cm

radially out from the center. Drilled holes were offset from one another by an angle of 15 degrees.

The sandstone disk was machined circular and ground flat at 2 cm thick. Holes were drilled at levels 2.7 mm, 6.1 mm, 9.9 mm, and 13.5 mm from the top (fracture) surface. The aluminum disk was prepared similarly, except its total thickness was a little greater than 2.5 cm with holes drilled at four even increments about 5.1 mm from the bottom to the top surface. The differences in rock/material preparation are illustrated in Figure 2.2.

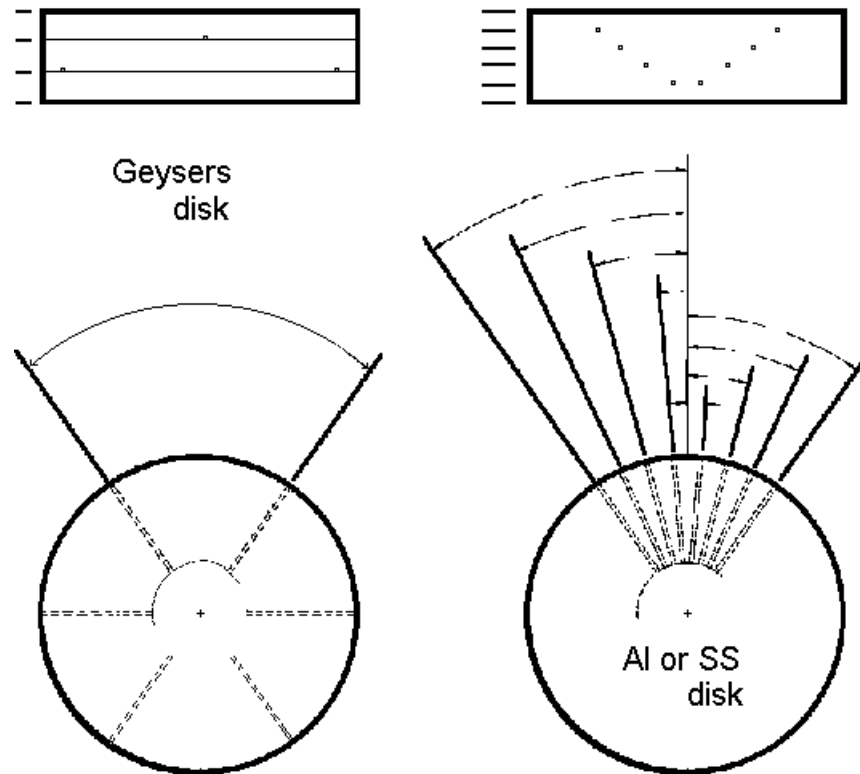


Figure 2.2: Comparison of thermocouple placement in graywacke (left) and sandstone and aluminum disks.

Thermocouples oriented in between the thin graywacke disks exhibited a suboptimal fit. This may have allowed circulation of fluid around a given thermocouple, influencing the temperature data at that point. Thermocouples inserted directly into the recently used sandstone and aluminum disks achieved a tight fit, as 1.000 mm diameter thermocouples were inserted in holes drilled with a 1.041 mm diameter drillbit.

2.3 FUTURE WORK

Another length of Geysers core has been requested for use in rerunning the experiment with a graywacke disk prepared similarly to the sandstone and aluminum disks. The new

graywacke disk will be prepared using a surface grinder, and drilled to specifications. Figure 2.3 illustrates the planned orientation of drilled holes to accommodate thermocouples with an exact fit.

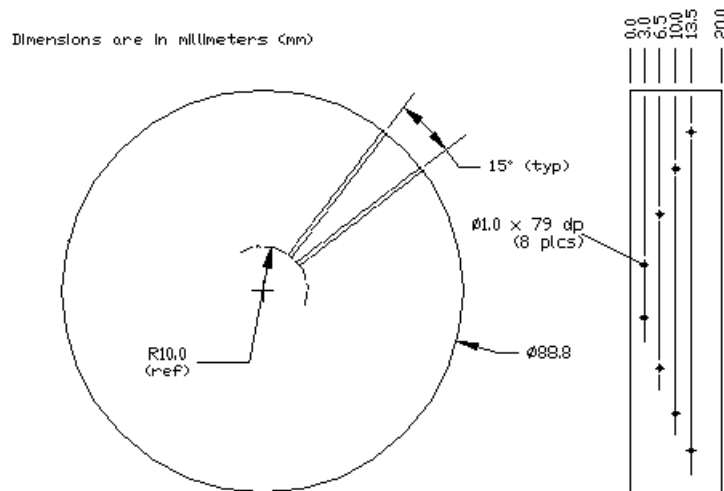


Figure 2.3: Thermocouple placement for graywacke disk in upcoming experiment.

The experimental apparatus will be reassembled with the graywacke disk. The heat flux sensors installed for this experiment will be checked and calibrated, as will the Data Acquisition System. This should eliminate the problems experienced in the previous experiments which involved heat flux sensor malfunction and incomplete data. The experiment will then be rerun using the same experimental procedure as was previously employed.

Previous experimental results indicated that low porosity and low permeability Geysers graywacke behaves unlike the sandstone or aluminum. The temperature gradient indicated that vaporization occurred beneath the fracture surface, isolating the boiling in the pores from the flow conditions in the fracture. Although this general behavior is again expected, the temperature gradients may exhibit a refined degree of accuracy unrealized in the original experiment. Additionally, a clearer relationship between observed behavior and collected data will be available for comparison between all three experimental materials.

3. INFERRING ENDPOINT SATURATION FROM BOILING EXPERIMENTS AND FIELD MEASUREMENTS

This project is being conducted by Research Assistant, Rodolfo Belen, Jr. and Prof. Roland Horne. The aim is to determine the endpoint saturation of steam and liquid water relative permeability curves of geothermal reservoir rocks.

3.1 INTRODUCTION

Relative permeability is important in describing the flow of two-phase steam in geothermal reservoirs. Presently, however, relative permeability relations for steam and liquid water are not completely understood. Permeability relations are normally adopted from field data or from nitrogen and water flow experiments.

The experimental determination of steam and liquid water relative permeabilities is a central target of the Stanford Geothermal Program. Experiments on Berea sandstones that were performed by Ambusso (1996) and Satik (1998) made use of X-ray computer tomography to determine steam saturation profiles. In a different approach, numerical simulation was used by Guerrero, Satik and Horne (1998) to infer relative permeabilities of Berea sandstones, based on temperature, pressure, heat flux and steam saturation data obtained from steady state boiling experiments performed by Satik (1997). Flow-through experiments are currently being performed by Mahiya (see Section 1) to measure steam and liquid water relative permeability relations and establish the repeatability of experimental results.

All of these earlier studies used Berea sandstone in order to capitalize on the larger permeability, which enabled the experiments to be performed in reasonable time. This study aims to extend the understanding to low permeability geothermal rocks by determining just the endpoint saturations of the relative permeability curves. The endpoint or irreducible or immobile saturation of a certain phase is the saturation at which that phase becomes mobile in multiphase flow.

Combining information about the endpoint saturations from the “slow” geothermal rock experiments with information about the general shape of the relative permeability curves from the “faster” sandstone rock experiments will completely define the steam-liquid water relative permeability behavior. Furthermore, determination of the irreducible water saturation will provide a better understanding of the adsorption characteristics and fluid storage capacities of geothermal rocks. This will be valuable in accurately estimating reserves of vapor-dominated geothermal fields such as the Geysers.

The objective of this study is to determine the endpoint saturation of the steam-liquid water relative permeability curves of geothermal rocks by experimentation and by inference from field measurements.

3.2 INFERRING ENDPOINT SATURATION FROM BOILING EXPERIMENTS

3.2.1 Experimental Design of Boiling Experiments

Before proceeding in designing an apparatus and procedures for the experimental determination of endpoint saturations, the results of previous steady state boiling experiments performed by Satik were first analyzed to check if endpoint saturations could be deduced from the experimental data obtained.

In 1996 and 1997, Satik performed a series of boiling experiments using Berea sandstone cores. The objective of the study was to improve on the understanding of the boiling process in porous media and to ultimately obtain capillary functions and relative permeability relations for steam and liquid water. The steady-state boiling experiments involved the heating of a rock saturated with liquid water and observing the boiling process by continuous measurement of pressure, temperature, heat flux and steam saturation within the rock. The X-ray CT scanner was used to visualize the boiling process and to determine the three-dimensional fluid distributions within the rock.

These experiments are analogous to drainage experiments in oil and water systems wherein the non-wetting fluid, oil, is injected into a rock saturated with the wetting fluid, water, to displace the water from the rock. However, in the case of the boiling experiments, steam produced by heating the water-saturated rock displaces the liquid water from the rock.

The experimental set-up consisted of a core holder housing the Berea sandstone core, a data acquisition system, a vacuum pump, a water pump and a balance (Figure 3.1).

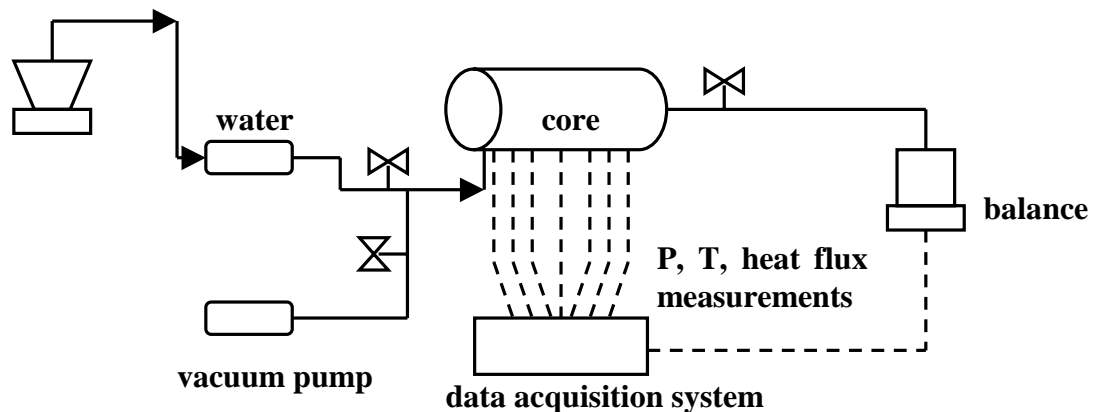


Figure 3.1: Experimental set-up of boiling experiments.

The core was insulated with a fiber blanket to minimize heat losses. The heater was attached to one end of the core that was closed to fluid flow. The other end was connected to a water reservoir placed on a balance that was used to monitor the amount of water displaced from the core during the boiling process. Pressure, temperature and heat

flux were measured in the core using pressure transducers, thermocouples and heat flux sensors respectively and were automatically recorded in a data acquisition system.

The core was first dried and then vacuumed to remove air inside the pore spaces. The core was then scanned at predetermined locations to obtain dry-core CT values that will be used in computing for the steam saturations. The core was then saturated with deaerated water and then scanned again to obtain wet-core CT values. The heater was then turned on and pressure, temperature and heat flux were continuously measured during each heating step until steady-state conditions were reached. Steady state has been reached when no more water flows out of the core and when pressure, temperature and heat flux measurements have stabilized. At the same time, the core was scanned again to obtain CT values that were used to calculate the steam saturation distribution. The heating rate was increased and the procedure was repeated. Several experiments were performed in which the core was mounted vertically and horizontally.

3.2.2 Discussion of Results

It was observed that as the heating rate was increased, the steady-state steam saturation data indicated a progressive boiling process with the formation of distinct regions of steam, two-phase and liquid water. Figures 3.2 to 3.4 are the steam saturation, pressure and temperature profiles of a bottom-heating vertical boiling experiment performed by Satik (1997) showing the formation of two-phase and liquid regions within the core as the boiling experiment progressed.

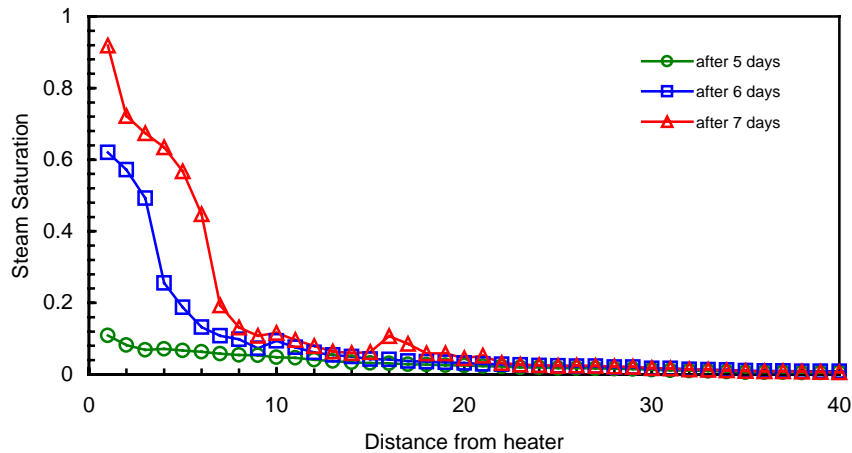


Figure 3.2: Steam saturation profile with time and distance from heater (Satik 1997).

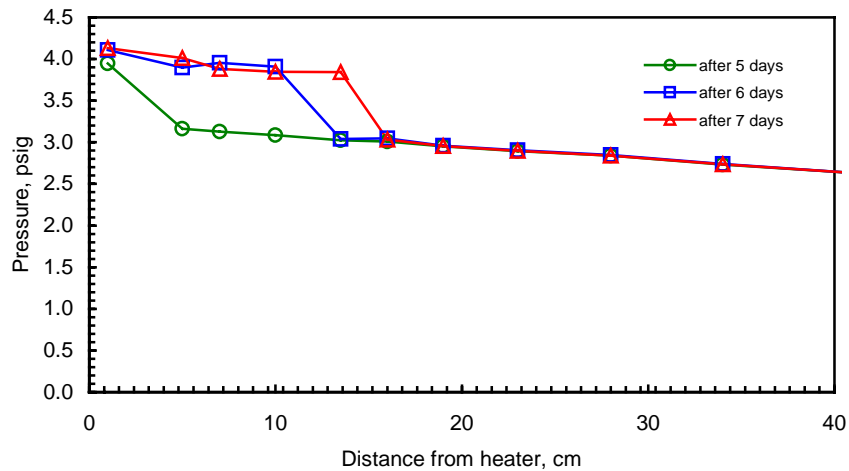


Figure 3.3: Pressure profile with time and distance from heater (Satik 1997).

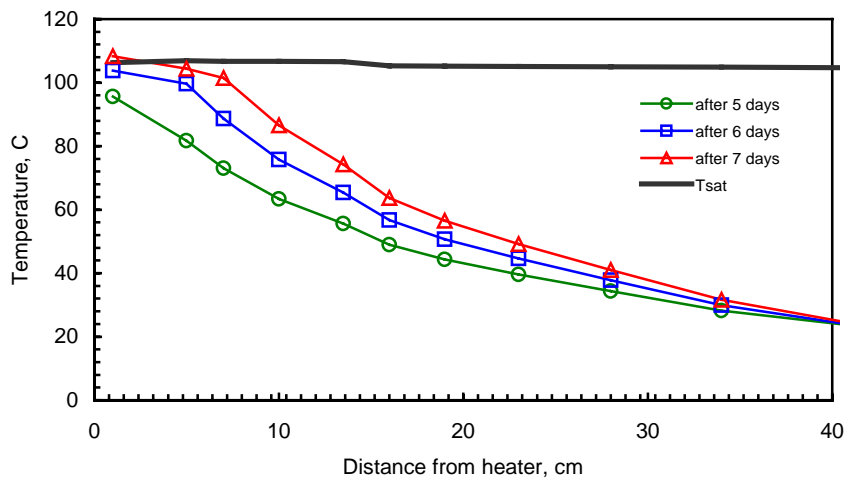


Figure 3.4: Temperature profile with time and distance from heater (Satik 1997).

Based on the experimental results, it is hypothesized that the irreducible water saturation can be inferred from the steam saturation profile. The elbow in the steam saturation profile in the core marking the transition from steam to two-phase conditions may indicate the value of the irreducible water saturation. This hypothesis was then tested by analyzing the sensitivity of the boiling process to the irreducible water saturation through numerical modeling. The boiling process was simulated using different values of endpoint saturation and the pressure, temperature and saturation profiles were predicted to verify if the elbow in the saturation profiles can be correlated with the irreducible water saturation. The two-dimensional radial iTOUGH2 model developed by Guerrero, et al. (1998) to infer relative permeability relations from the boiling experiment results was used in the sensitivity analysis. The simulation was done by performing forward calculations in iTOUGH2.

Figures 3.5 to 3.8 show the preliminary results of the forward calculation runs performed using linear and Corey relative permeability relations and Leverett capillary functions. These simulation results correspond to pressure, temperature, and saturation profiles after seven days of experiment time.

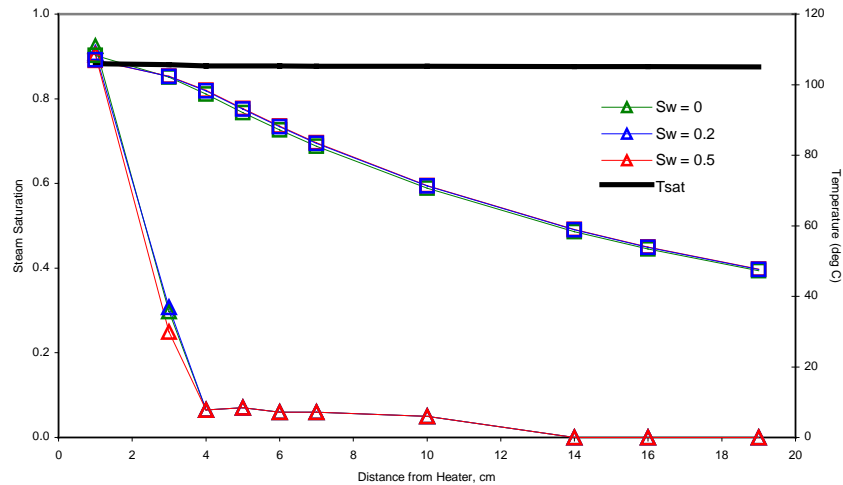


Figure 3.5: Steam saturation and temperature profiles using Corey relative permeability relation and Leverett capillary function.

Based on the preliminary results using the Corey relative permeability relation, it appears that the boiling process is not strongly sensitive to the irreducible water saturation. Varying the endpoint water saturation did not significantly change the pressure, temperature, and saturation profiles in the core particularly in the two-phase region. On the other hand, the forward calculation results using the linear relative permeability relation show an apparent correlation between the elbow in the saturation profile and the irreducible water saturation as indicated by the simulated steam saturation 1 cm from the heater end (Figures 3.7 and 3.8). Further simulation will be done to confirm these observations.

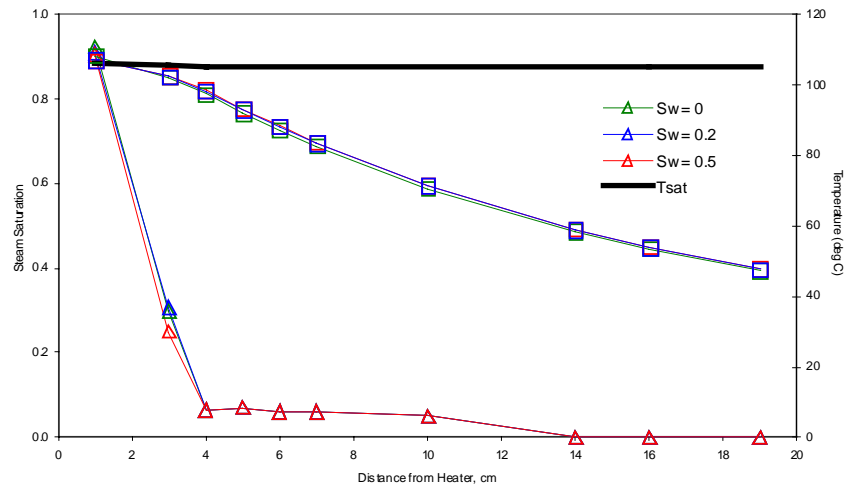


Figure 3.6: Steam saturation and pressure profiles using Corey relative permeability relation and Leverett capillary function.

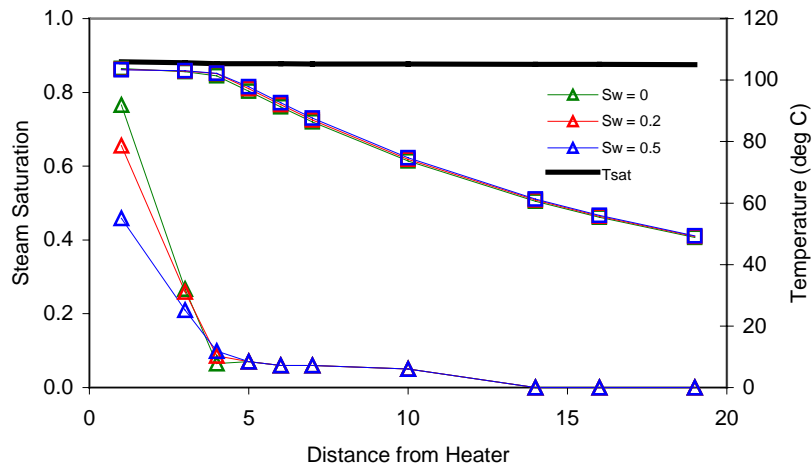


Figure 3.7. Steam saturation and temperature profiles using linear relative permeability relation and Leverett capillary function.

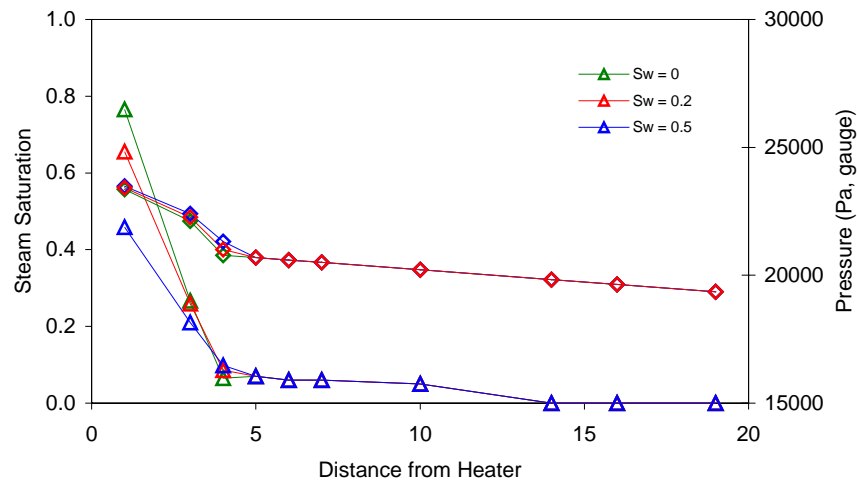


Figure 3.8: Steam saturation and pressure profiles using linear relative permeability relation and Leverett capillary function.

3.2.3 Future Work

Future work will involve further simulation using iTOUGH2, focusing on the determination of steam saturation profiles near the heater end of the core as well as profiles at later times. The model constructed by Guerrero, et al. had four concentric rings and 51 layers, each with a thickness of 1 cm. It is intended to decrease the grid block size and focus on the layers closest to the heater end where steam and two-phase conditions exist.

Furthermore, it is intended to run the forward calculations beyond the experiment time of seven days to determine the steam saturation profiles at later times when the steam and two-phase regions have expanded. This will verify if the elbow in the steam saturation profile corresponding to the irreducible water saturation will persist with time.

After confirming that the irreducible water saturation can be inferred from these boiling experiments, future work will be directed toward performing the boiling experiments using lower permeability rocks. The apparatus and procedures may then be modified if necessary.

3.3 INFERRING ENDPOINT SATURATION FROM FIELD MEASUREMENTS

3.3.1 Zero-Dimensional Model

Reservoir saturation can be inferred from the change in temperature accompanying production from a reservoir. The in-place water saturation can be estimated by solving the material and energy balance equations defining a simple zero-dimensional model of

the reservoir. This study aims to improve on this approach by extending the zero-dimensional model and considering transient and spatial effects.

Consider a reservoir with a volume, V , containing two-phase fluids initially at some temperature T_1 and reservoir saturation S_1 . The mass of the fluids initially in-place is given by the porosity, ϕ , reservoir volume, reservoir saturation, and the densities of the two phases, ρ_s and ρ_w . The mass of the reservoir rock is given by the porosity, reservoir volume and the rock density, ρ_r .

$$\text{mass of fluids in-place} = \phi V \rho_w S_1 + \phi V \rho_s (1 - S_1) \quad (3.1)$$

$$\text{mass of rock} = (1 - \phi) V \rho_r \quad (3.2)$$

Similarly, the energy of the fluids initially in-place is given by the mass and the specific enthalpy of the fluids, h_s and h_w . The energy contained in the rock is given by the mass, specific heat capacity, C_r , and the temperature of the rock. It is assumed that there is local thermal equilibrium between the reservoir fluids and rock.

$$\text{energy of fluids in-place} = \phi V \rho_w S_1 h_w + \phi V \rho_s (1 - S_1) h_s \quad (3.3)$$

$$\text{energy of rock} = (1 - \phi) V \rho_r C_r T_1 \quad (3.4)$$

Production from the reservoir causes the pressure and temperature of the reservoir to decrease and, consequently, some of the liquid water to flash. Consider that the temperature drops to T_2 and the water saturation to S_2 as a result of production. Performing material and energy balance around the reservoir gives the saturation of the reservoir and the mass of produced fluids assuming steady-state conditions have been reached.

Material Balance:

$$\Delta(\phi V \rho_w S) + \Delta(\phi V \rho_s [1 - S]) + m' = 0 \quad (3.5)$$

Energy Balance:

$$\Delta(\phi V \rho_w S h_w) + \Delta(\phi V \rho_s [1 - S] h_s) + (1 - \phi) V \rho_r C_r \Delta T + m' h' = 0 \quad (3.6)$$

where m' and h' are the mass and enthalpy of the fluids produced.

Solving the material and energy balance equations defined earlier gives a plot of the enthalpy of the production fluids as a function of the reservoir pressure drop and the reservoir saturation. Consider as an example a Geysers well with a shut-in downhole temperature of 240°C. Porosity of the reservoir rock is 5%, rock density is 1,750 kg/m³ and rock specific heat is 1 kJ/kgK. Figure 3.9 is the enthalpy and pressure drop plot for

the case of the Geysers example. This plot can be used as a diagnostic tool for estimating reservoir saturation based on production enthalpy and reservoir pressure data.

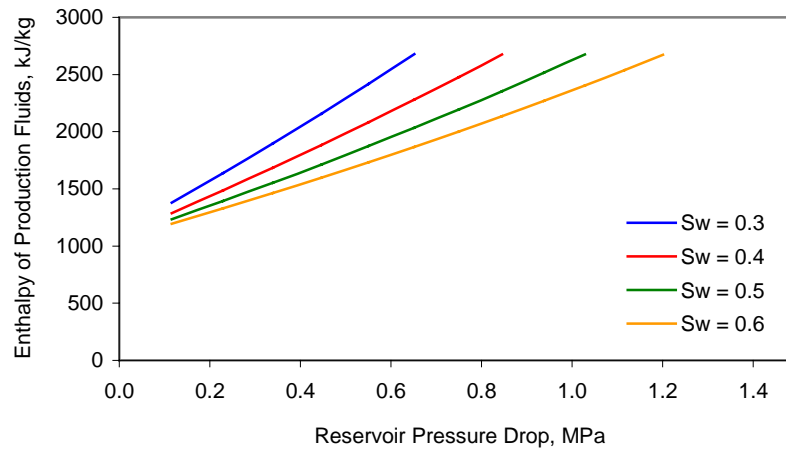


Figure 3.9. Enthalpy of production fluids as a function of reservoir pressure drop and reservoir saturation.

The simple zero-dimensional model of the reservoir can, therefore, be used to estimate the irreducible water saturation of geothermal reservoir rocks using field measurements of temperature and enthalpy. Consider again the Geysers well that produces 200°C dry saturated steam. The in-place water saturation calculated using material and energy balance equations is about 0.5, which corresponds to the irreducible water saturation of the reservoir rocks since the well is producing dry saturated steam.

3.3.2 Future Work

The zero-dimensional approach does not take into account pressure and enthalpy variations with time and distance. The model assumes that the reservoir has a uniform saturation and temperature. Future work will involve modeling of two-phase radial flow to obtain pressure and saturation profiles with time and radial distance. Modeling results will provide a deeper insight on the estimation of reservoir saturation using field measurements. Furthermore, it is also intended to perform simple laboratory scale flash experiments using water-saturated cores to determine the irreducible water saturation.

4. STEAM-WATER CAPILLARY PRESSURE

This project is being conducted by Research Associate Kewen Li and Professor Roland Horne. The aim of this project is to measure steam-water capillary pressure in geothermal rocks.

4.1 INTRODUCTION

Capillary pressure plays an important role in geothermal reservoirs. As an example, Urmeneta, et al. (1998) studied the role of capillary forces in the natural state of fractured geothermal reservoirs using numerical techniques and found that capillary pressure tended to keep the vapor phase in the fractures and the liquid phase in the matrix. The numerical results from Urmeneta, et al. (1998) showed that capillary forces control the transfer of fluids between fractures and matrix, the stability of liquid-dominated two-phase zone, and the distribution of steam and water in geothermal reservoirs. Hence, the value of capillary pressure may influence the estimation of reserve and production performance. Unfortunately, there are few experimental data of steam-water capillary pressure.

Sta. Maria and Pingol (1996) calculated the value of capillary pressure from the adsorption data of Horne, et al. (1995) and found the capillary pressure ranging from 0 to 586 MPa. Persoff and Hulen (1996) also inferred the capillary pressure from adsorption data of Geysers rock samples and found the capillary pressure ranging from 0 to 190 MPa. Melrose (1991) on the other hand, obtained a capillary pressure of up to 69 MPa by scaling down the data from three different methods: porous-plate, water adsorption/desorption, and mercury injection. These results show a lot of inconsistency. Therefore, it is necessary to develop a reliable technique to measure the capillary pressure directly.

In this report, we focus on the derivation of a new formula for calculating steam-water capillary pressures by water imbibition experiments. A linear correlation between imbibition rates of water and the reciprocal of imbibition recovery has been found theoretically. Capillary pressures may be calculated using the new correlation. Our experimental results confirmed the validity of the new developed theory to calculate capillary pressures from water imbibition experiments.

4.2 THEORY

Spontaneous imbibition of water into a gas-saturated rock may be considered as a capillary pressure-dominated process. Assuming that a natural rock is water-wet in a gas-water system, water imbibes into the gas-saturated rock when its bottom touches the water surface as shown in Figure 4.1.

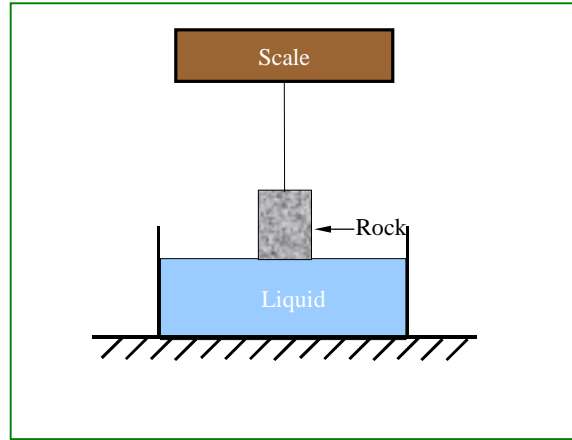


Figure 4.1: Schematic of water imbibition experiment.

In this case, capillary pressure is the driving force against gravity that pulls water into the liquid-wet rock. Therefore, it is possible to infer capillary pressure from one spontaneous imbibition test of water into a gas-saturated rock.

Applying Darcy's equation to the process of the spontaneous imbibition that occurs vertically upward as shown in Figure 4.1, the imbibition velocity of water is expressed as:

$$v_w = -\frac{k_w}{\mu_w} \left(\frac{\partial p_w}{\partial x} + \rho_w g \right), \quad (4.1)$$

where v_w and k_w are the flowing velocity and the effective permeability of water phase, respectively; ρ_w and μ_w are water density and viscosity; p_w is the pressure of water phase at the position x . From the definition of capillary pressure, the pressure of water phase can be calculated:

$$p_w = p_g - p_c, \quad (4.2)$$

Substituting Equation 4.2 into Equation 4.1:

$$v_w = \frac{k_w}{\mu_w} \left(\frac{\partial p_c}{\partial x} - \frac{\partial p_g}{\partial x} - \rho_w g \right), \quad (4.3)$$

where p_g is the pressure of gas phase and p_c is capillary pressure.

Usually, gas mobility is much greater than water mobility. If gas mobility is assumed to be infinite, gas pressure gradient is estimated as:

$$\frac{\partial p_g}{\partial x} = -\rho_g g, \quad (4.4)$$

where ρ_g is gas density. Substituting Equation 4.4 into Equation 4.3:

$$v_w = \frac{k_w}{\mu_w} \left(\frac{\partial p_c}{\partial x} - \Delta\rho g \right), \quad (4.5)$$

where $\Delta\rho$ is the density difference between gas and water.

Schembre, et al. (1998) used the X-ray CT method to monitor the process of water imbibition into air-saturated rocks that were assembled vertically; they reported that the CT images of diatomites and chalk showed a homogeneous and piston-like water front during the water imbibition. Our experimental results that will be discussed in the next section also showed that water imbibition is a piston-like flow process. Based on these experimental observations, water does imbibe into air-saturated rocks in a piston-like manner in certain cases. The following equations describe a piston-like flow:

$$\frac{\partial p_c}{\partial x} = \frac{p_c}{x}, \quad (4.6)$$

$$N_{wt} = Ax\phi S_w, \quad (4.7)$$

where A and N_{wt} are the cross-section area of the core and the volume of water imbibed into the core, respectively; ϕ is porosity and S_w is the water saturation behind the water front in the core. The water imbibition velocity can be expressed as:

$$v_w = \frac{dx}{dt}, \quad (4.8)$$

Using Equations 4.6, 4.7, 4.8, Equation 4.5 is reduced:

$$\frac{dN_{wt}}{dt} = a \frac{1}{\eta} - b, \quad (4.9)$$

where:

$$a = \frac{Ak_w S_w}{\mu_w L} p_c, \quad (4.10)$$

$$b = \frac{Ak_w}{\mu_w} \Delta \rho g, \quad (4.11)$$

and

$$\eta = \frac{N_{wt}}{V_p}, \quad (4.12)$$

where V_p and L are the length and the pore volume of the core sample, respectively; η is the cumulative fraction of gas recovered.

If a and b are constants, their values can be obtained from the plot of imbibition rate vs. $1/\eta$. Capillary pressure is then calculated using Equation 4.10 with the value of k_w computed by Equation 4.11. Are a and b constants? If a linear correlation exists between the experimental data of imbibition rate and $1/\eta$, we may prove that a and b are constants. What are k_w and p_c in Equation 4.10 exactly? In the related literature, k_w and p_c are defined as the effective permeability of water and capillary pressure. Defining k_w and p_c like this may not be enough. In this study, clear definitions for k_w and p_c are required. In Equation 4.10, k_w is the effective water permeability at S_w , that is the mean water saturation behind the water front; p_c is the maximum imbibition capillary pressure at zero water saturation (if the rock is initially saturated with gas completely) instead of S_w . If the rock is initially saturated with water at an initial water saturation of S_{wi} , p_c is the maximum imbibition capillary pressure at a water saturation of S_{wi} . Therefore, if we do the water imbibition experiments at different initial water saturations, a capillary pressure function of water saturation may be obtained.

4.3 EXPERIMENTS

Brine of 1.0 percent (wt) NaCl was used as the liquid phase and air the gas phase in the imbibition experiments for measuring air-water capillary pressure; the specific gravity and viscosity of the brine were 1.01 and 1.0 cp at 20°C.

Berea was used as the rock in this study. The permeability and porosity of the rock are 600.0 md and 20.4%; its length and diameter are 43.2 cm and 5.08 cm, respectively.

The schematic of the apparatus for doing water imbibition is shown in Figure 4.1. The core sample hangs under a balance with an accuracy of 0.1 g. The amount of water imbibed into the core with time is recorded by the balance.

The core sample was dried by heating at a temperature of 85°C in an air bath until its weight did not vary during eight hours. The core sample was assembled in the apparatus as shown in Figure 4.1 after it was cooled down. Water started to imbibe into the core when its bottom was brought into contact with the water surface by raising the water container. The weight change of the core sample with time was then recorded and used to calculate capillary pressure.

4.4 RESULTS

Figure 4.2 shows the experimental results of water imbibition into an air-saturated rock. The amount of water imbibition, imbibition recovery, is represented by the volume of water imbibed into the rock divided by the pore volume of the core.

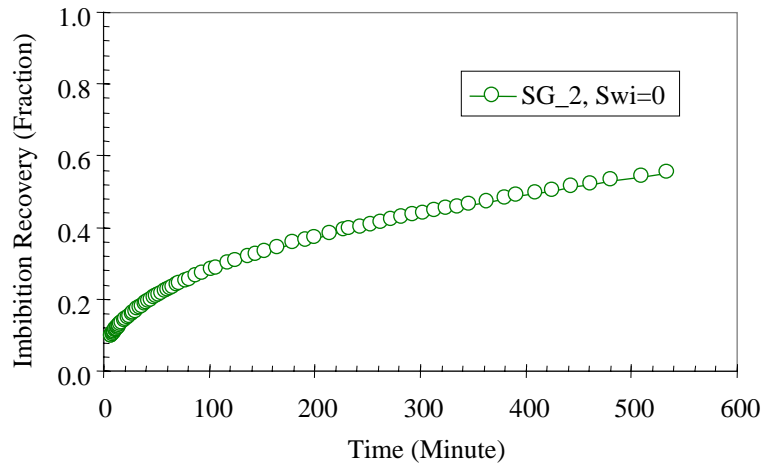


Figure 4.2: Water imbibition recovery with time.

The relationship between the imbibition rate of water and the reciprocal of imbibition recovery is plotted in Figure 4.3. It is observed in this figure that a linear correlation does exist between the imbibition rate of water and the reciprocal of imbibition recovery as predicted from Equation 4.9.

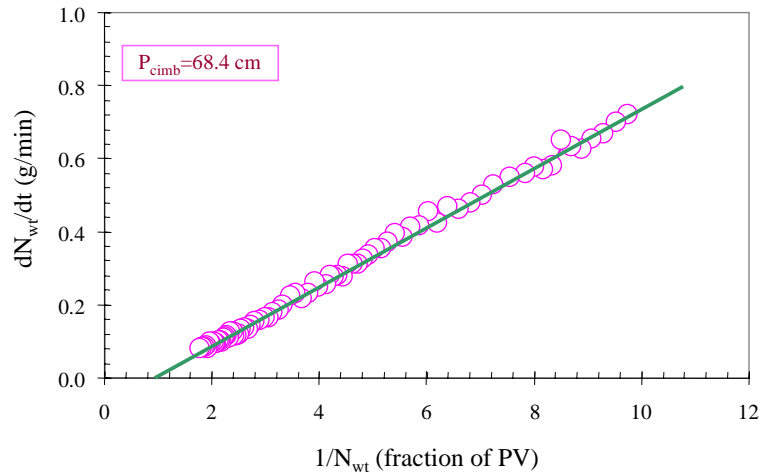


Figure 4.3: Imbibition rate vs. reciprocal of recovery.

The linearity shown in Figure 4.3 also demonstrates that a and b are constants. Meanwhile, a and b being constant seems to prove that the water imbibition into an air-saturated rock is a piston-like process. Therefore, our present experimental results confirmed the validity of the new developed theory for calculating capillary pressure from spontaneous water imbibition tests.

The computed maximum capillary pressure at zero water saturation is about 68.4 cm of water column, which implies that water can climb to a height of 68.4 cm in the air-saturated core with a permeability of about 600 md.

4.5 CONCLUSIONS

1. A new method was developed for characterizing the spontaneous imbibition in gas-liquid systems.
2. Capillary pressure may be calculated from one imbibition test for steam-water systems.
3. The new method is of importance for the scaling of experimental imbibition data.

4.6 FUTURE WORK

We will do water imbibition experiments in air-water systems at different initial water saturations and calculate the capillary pressure in order to verify further the feasibility of this new method. We will also use X-ray CT method to measure the water saturation distribution in a vertical sand pack and obtain the capillary pressure curve. We will then compare capillary pressure curves measured by imbibition tests and the CT method. Once these procedures have been verified, we will move on to consider geothermal rocks.

5. SLIP EFFECT IN STEAM FLOW

This project is being conducted by Research Associate Kewen Li and Professor Roland Horne. The aim is to study the effect of gas slippage on steam-water relative permeabilities and to develop a method for accurately measuring the slip effect in steam flow.

5.1 SUMMARY

The accurate estimation of steam flow properties is important for geothermal reservoir engineering and the numerical simulation of reservoir performance. It has been found that the steam phase relative permeabilities at some water saturations may be significantly greater than one. This unexpected observation has been interpreted physically and reproduced in nitrogen-brine flow. A new method for measuring and correcting gas-liquid relative permeabilities has been developed. The unusual values of gas phase or steam phase relative permeabilities were found to be attributable to the gas slip (Klinkenberg) effect. The effect of water saturation on gas slippage has been investigated; experimental results show that water saturation has a significant influence on the gas slippage.

5.2 INTRODUCTION

Steam-water relative permeabilities are fundamental properties in reservoir engineering and numerical simulation for geothermal reservoirs. There are only a few measurements of steam-water relative permeabilities reported in the literature, and published values are frequently inconsistent. The main difficulties in making steam-water relative permeability measurements arise from the following four aspects: 1) mass transfer between phases makes it difficult to measure or calculate fractional flow; 2) extremely low permeabilities of geothermal rocks; 3) difficulties in measuring heat loss during experiments; 4) unclear mechanisms of gas-liquid flow. For example, the effect of gas slippage (Klinkenberg effect) on gas phase relative permeabilities in steam-water two-phase flow is not clear; very few studies related to the gas slip effect in steam-water flow have been published.

Satik and Horne (1998) observed an unusual phenomenon in that steam-water relative permeabilities (k_{rg}), at some water saturations sometimes appear to be greater than 1.0 (see Figure 5.1). A similar phenomenon was also found in a recent experiment conducted by Mahiya (1999) as described in Section 1 of this report. What causes the steam phase relative permeabilities greater than 1.0? Steam is subject to a prominent flow characteristic of gas molecules, namely the gas slippage or Klinkenberg effect. Gas permeability k_g at a low mean pressure is greater than the absolute liquid permeability (k) due to the gas slip effect. If the gas slippage is large enough, the gas permeability at low water saturation may still be greater than the absolute permeability. From the definition of relative permeability, k_g/k , the gas relative permeability may be greater than one. Hence the phenomenon of gas slippage may be the reason steam-water relative permeability experiments have shown values of k_{rg} greater than one.

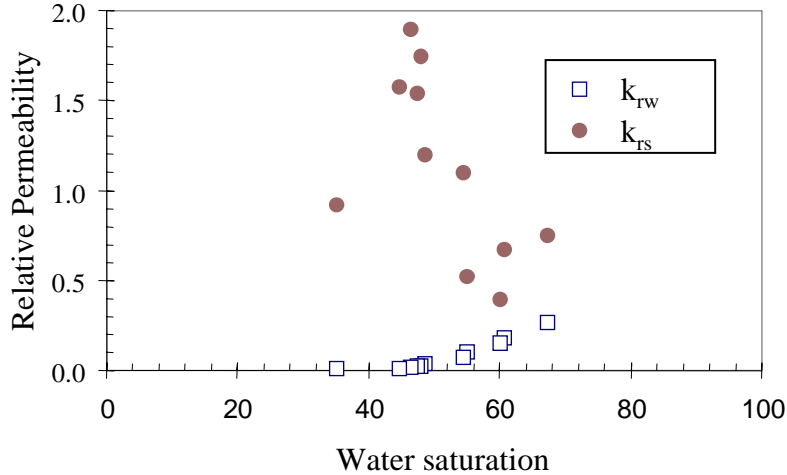


Figure 5.1: Steam-water relative permeabilities (from Satik and Horne 1998).

The gas slippage theory established by Klinkenberg (1941) in single-phase gas flow is expressed as follows:

$$k_g = k_{g\infty} \left(1 + b \frac{1}{p_m}\right), \quad (5.1)$$

where k_g is the gas permeability at a mean pressure, p_m , and $k_{g\infty}$ the intrinsic permeability of gas at an infinite pressure, respectively; b is the gas slip factor. The mean pressure is defined by $p_m = (p_i + p_o) / 2$; p_i and p_o are inlet and outlet pressures of the cores, respectively.

Jones and Owens (1980) measured the gas permeabilities on more than 100 tight gas sand samples with permeabilities ranging from 0.0001 to 1.0 md and their data yielded a relationship between b and $k_{g\infty}$ for single-phase gas flow:

$$b = 0.86k_{g\infty}^{-0.33}, \quad (5.2)$$

Sampath and Keighin (1982) thought that a correlation, if it exists, should be between b and $k_{g\infty}/\phi$ rather than between b and $k_{g\infty}$; they suggested a correlation between the gas slip factor and the intrinsic gas permeabilities based on their experimental results using nitrogen:

$$b = 0.0955(k_{g\infty} / \phi)^{-0.53}, \quad (5.3)$$

where ϕ is the porosity of the core sample. Sampath and Keighin (1982) found that the intrinsic gas permeabilities decrease with increasing partial water saturations.

Council (1979) discussed gas slip effect and showed that the effect of gas slippage was small when $b = 0.2$ atm and $p_m = 10$ atm. So the gas slip effect was not considered in the analysis of the gas flow data. Council (1979) stated that “For the case of steam-water relative permeabilities, slip could be reduced by running experiments at very high pressures, and therefore very high temperatures.” There are certain difficulties in running experiments at very high pressures and temperatures for measuring steam-water relative permeabilities, for example, when the X-ray CT method is used to measure the water saturation in a core (Ambusso, et al., 1996). On the other hand, increasing experimental temperature will increase the value of b significantly as reported by Wel, et al. (1986). Increasing b will increase the influence of gas slippage on steam flow properties.

Geothermal rock often has a very low intrinsic permeability in an order of 10^{-6} d. The value of b computed using Equation 5.2 is about 82.1 atm for this permeability. The mean pressure should be equal to about 1000 atm so as to neglect the gas slip effect in single-phase gas flow. In two-phase flow, the mean pressure necessary to neglect the gas slip effect is greater than that in single-phase gas flow. Obviously, it is not easy to operate experiments at pressures over 1000 atm. It can be seen from this simple calculation that the effect of gas slippage on steam flow properties may be very significant in geothermal reservoirs.

Herkelrath, et al. (1983) recognized the importance of gas slippage and incorporated it into a single-phase steam flow model in order to model steam pressure-transient experimental data. In their study, the gas slip factor measured using nitrogen gas was assumed to apply to the steam flow.

Hence it is seen that it is necessary to measure the slip factor of steam flow in a porous medium in order to obtain reliable relative permeability data for steam. When the data of steam slip factor are available, it will be possible to determine how important the steam slip effect is in steam-water two-phase flow.

In this work, an apparatus was developed for measuring gas-liquid relative permeability using an on-line weighing method with a balance. A new procedure for measuring and correcting gas relative permeabilities was proposed. The effects of water saturation on the gas slip factor and the intrinsic gas permeabilities were also investigated.

5.3 THEORY

Assuming that Darcy’s equation is valid for steam-water two-phase flow and that capillary pressures are neglected, the effective permeability of steam phase is calculated using the following equation:

$$k_s(S_w) = \frac{q_s \mu_s L p_o}{A \Delta p p_m}, \quad (5.4)$$

where $k_s(S_w)$ is the effective steam phase permeability at a water saturation of S_w ; q_s and μ_s are the flow rate and viscosity of steam phase; Δp is the differential pressure across the core sample; A and L are the cross-section area and the length of the core sample. The relative permeability of steam phase is usually calculated without the correction of steam slip effect as follows:

$$k_{rs}(S_w) = \frac{k_s(S_w)}{k}, \quad (5.5)$$

where $k_{rs}(S_w)$ is the relative permeability of steam phase at water saturation of S_w ; k is the absolute permeability of the rock sample.

With consideration of the steam slip effect, the intrinsic effective permeability of the steam phase is calculated using the following formula:

$$k_{s\infty}(S_w) = \frac{k_s(S_w)}{(1 + b_{S_w} / p_m)}, \quad (5.6)$$

where $k_{s\infty}(S_w)$ and b_{S_w} are the intrinsic effective permeability and the slip factor of steam phase at a water saturation of S_w . Hence the relative permeability of steam phase with steam slip effect included is calculated using the following equation:

$$k_{rs\infty}(S_w) = \frac{k_{s\infty}(S_w)}{k}, \quad (5.7)$$

where $k_{rs\infty}(S_w)$ is independent of test pressure and will be named the no-slip relative permeability of steam phase at a water saturation of S_w .

It is seen from Equation 5.6 that the essential issue for calculating the no-slip relative permeability of steam phase is to measure the value of b_{S_w} , the slip factor of steam phase at a water saturation of S_w .

A steady-state method as illustrated in Figure 5.2 was used to measure the relative permeabilities of nitrogen-water, from which gas phase relative permeabilities were calculated using the methods described by Equations 5.5 to 5.7 for the steam phase. Water phase relative permeabilities can be calculated directly using Darcy's equation. The corresponding water saturations were calculated using either of the two balances in the apparatus (see Figure 5.2):

$$S_{w,i+1} = S_{w,i} - \frac{\Delta M_{i1}}{V_p \rho_w}, \quad (\text{using Balance 1}) \quad (5.8)$$

or

$$S_{w,i+1} = S_{w,i} + \frac{\Delta M_{i2}}{V_p \rho_w}, \text{ (using Balance 2)} \quad (5.9)$$

where V_p is the pore volume of the core sample; $S_{w,i}$ and $S_{w,i+1}$ are the water saturations at i^{th} and $i+1^{\text{th}}$ points, respectively; ΔM_{i1} and ΔM_{i2} are the weight variations recorded by Balances 1 and 2, respectively; ρ_w is the water density.

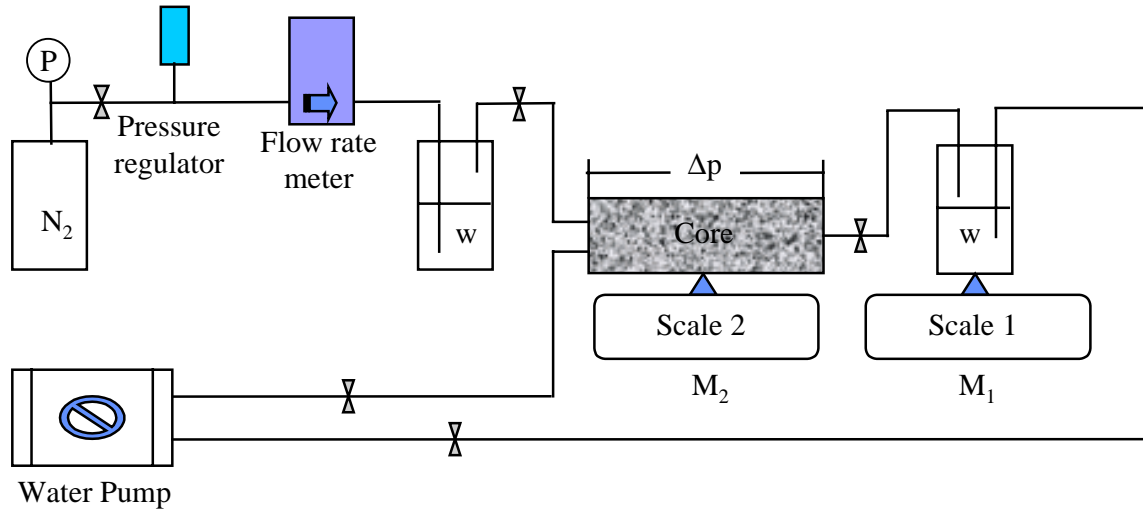


Figure 5.2: Schematic of gas-water relative permeability steady-state test.

5.4 EXPERIMENTS

Brine of 1.0 percent (wt) NaCl was used as the liquid phase and nitrogen the gas phase in the experiments for measuring nitrogen-water relative permeabilities; the brine specific gravity and viscosity were 1.01 and 1.0 cp at 20°C.

Berea was used in this study in order to investigate the effect of gas slippage on the gas relative permeabilities in gas-liquid two-phase flow. The permeability and porosity of the rock are 1280 md and 23.4%, respectively; the length and diameter are 43.2 cm and 5.08 cm, respectively.

The schematic of the apparatus for measuring nitrogen-water relative permeabilities using a steady-state method is shown in Figure 5.2. For the water phase, the system is closed. So the decrease (or increase) of water volume in the core is equal to the increase (or decrease) of water volume in the container at the core outlet on Balance 1 (assuming that the water phase is incompressible). Balance 1 has an accuracy of 0.01 g. Water saturations in the core are then calculated using the data from Balance 1. In order to develop a method for measuring water saturations in cores at high temperatures for steam-water two-phase flow systems, another balance (Balance 2 in Figure 5.2) was used to weigh the coreholder directly. Flexible tubings for fluid injection at the inlet and for

production at the outlet were used to connect to the core so that the decrease (or increase) of the coreholder weight would be directly proportional to the decrease (or increase) of water saturations in the core. Therefore, the water saturations in the core could also be measured by Balance 2; this balance has an accuracy of 0.1 g. The water saturations measured by the two balances should be equal to each other.

The core sample was first dried by evacuation. The weight of the coreholder was monitored using a balance with an accuracy of 0.1 g. The core was assumed to be dry when its weight did not change in eight hours of evacuation at a vacuum of about 30 millitorr. Then the gas permeabilities were measured at different mean pressures using nitrogen. Following that, the core was completely saturated with 1% (wt) NaCl brine by evacuation and the absolute liquid permeability of the core was measured after several pore volumes of brine were injected. Next, steady-state relative permeability experiments were started and varying fractions of nitrogen and water were injected into the core. Measurements at each fraction resulted in a single data point on a relative permeability vs. water saturation curve. In this study, the experiment commenced from a water saturation of 100%. The water saturations were reduced by increasing the fraction of gas in the injected fluids, which formed a drainage relative permeability curve. Subsequently the opposite procedure with decreasing water saturations formed an imbibition curve.

5.5 EXPERIMENTAL RESULTS

Nitrogen-water two-phase relative permeabilities were measured at ambient conditions. It was found that some relative permeabilities of the gas phase were greater than 1.0 at certain low water saturations due to gas slippage. The experimental results are discussed in this section.

Figure 5.3 shows the relationship between the gas permeabilities and the reciprocal of mean pressure across the core sample at different water saturations ranging from zero to 31.8%. It can be seen from Figure 5.3 that a linear correlation between the gas permeabilities and the reciprocal of mean pressure exists at all the tested water saturations. The intrinsic gas permeability at zero water saturation is calculated by a linear regression on the experimental data. The computed intrinsic gas (nitrogen) permeability, that is, the gas permeability corresponding to an infinite pressure, $k_{g\infty}$, is equal to 1274.5 md and close to the absolute liquid permeability of 1280.0 md measured using 1% (wt) NaCl brine. The gas slip factor at zero water saturation is about 0.45 atm. It can be also seen from Figure 5.3 that the water saturation has a significant effect on the intrinsic effective gas permeability.

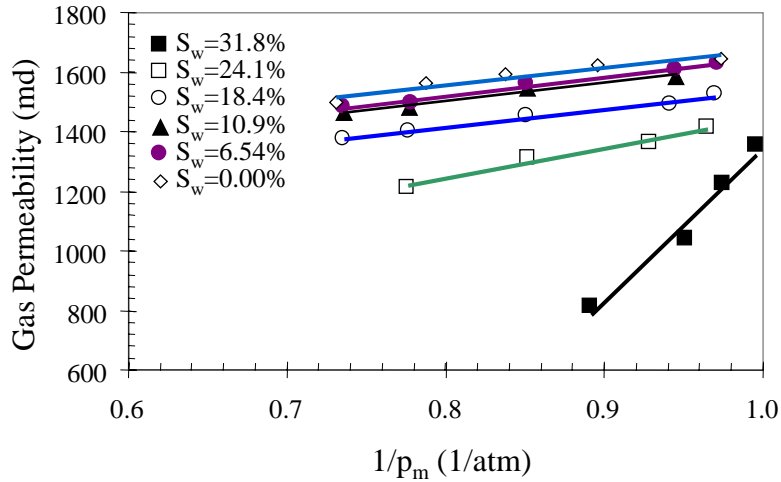


Figure 5.3: Slip effect at different water saturations.

Figure 5.4 plots the computed gas slip factors at different water saturations vs. the corresponding intrinsic effective gas permeabilities at different water saturations. A linear relationship between the gas slip factor and the intrinsic effective gas permeability at different water saturations is observed on a log-log plot in Figure 5.4. This work seems to be reasonable according to Equation 5.2 even though Equation 5.2 is based on the experimental results for single-phase gas flow.

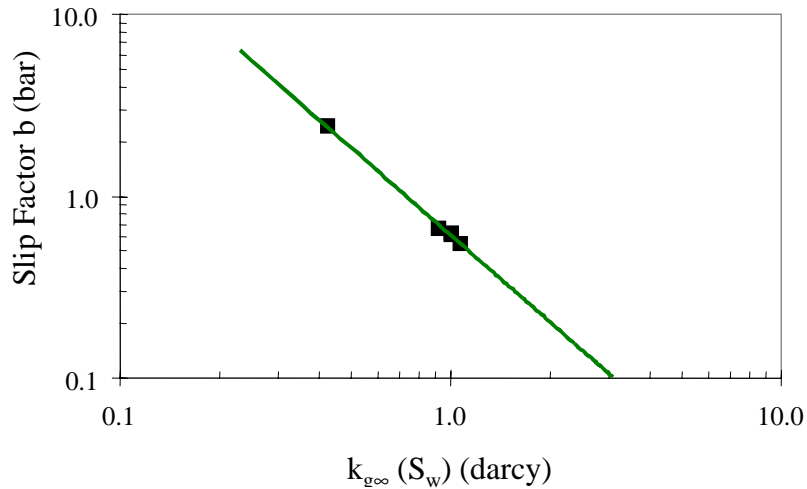


Figure 5.4: Correlation between b and $k_{g\infty}(S_w)$.

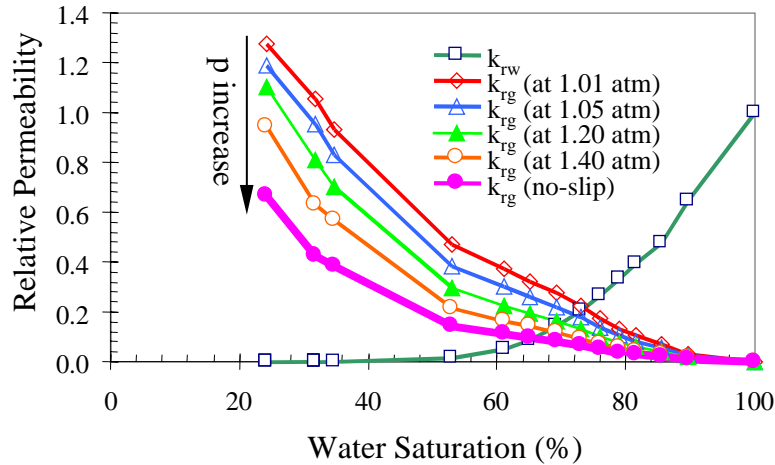


Figure 5.5: Gas-water relative permeabilities at different pressures.

The experimental gas-water relative permeabilities for the drainage process are shown in Figure 5.5; this figure demonstrates that gas relative permeability increases with decreasing mean pressure and may be greater than 1.0 at some low water saturations due to the gas slip effect. The no-slip relative permeabilities of the gas phase are calculated using Equation 5.7 and plotted in Figure 5.5 as solid circles. It can be seen from Figure 5.5 that the corrected no-slip relative permeabilities of gas phase are always less than 1.0. The gas relative permeabilities at any mean pressure may be computed using Equations 5.5-5.7 once the no-slip relative permeabilities of gas phase and the gas slip factors at different water saturations are available.

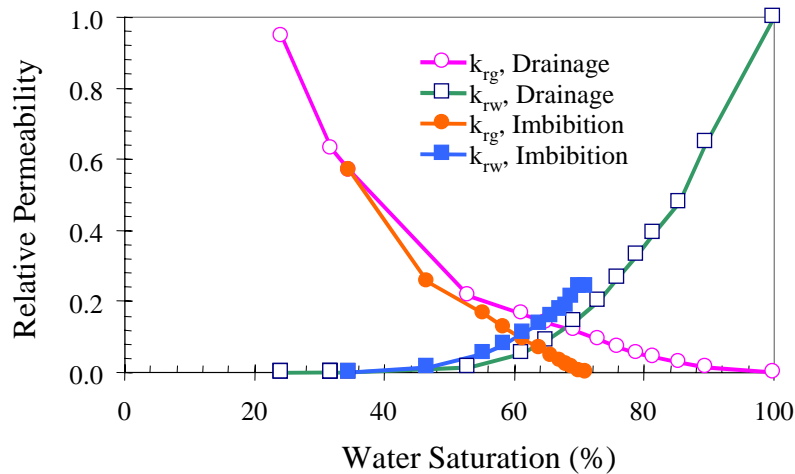


Figure 5.6: Imbibition and drainage gas-water relative permeabilities (without correction of gas slippage).

The gas-water relative permeabilities for the imbibition process were also measured following the drainage process. The water saturation was increased in the imbibition process by decreasing the gas flow rate and increasing the water flow rate. Figure 5.6 shows the gas-water relative permeabilities at a mean pressure of about 1.4 atm for the imbibition process without correcting the gas slip effect.

The drainage water relative permeabilities are a little less than those of imbibition; the gas relative permeabilities of drainage are greater than those of imbibition.

The no-slip gas relative permeabilities for both imbibition and drainage are shown in Figure 5.7. It can be seen from Figures 5.6 and 5.7 that the no-slip gas relative permeabilities of both imbibition and drainage processes are less than the values obtained without correcting the gas slip effect.

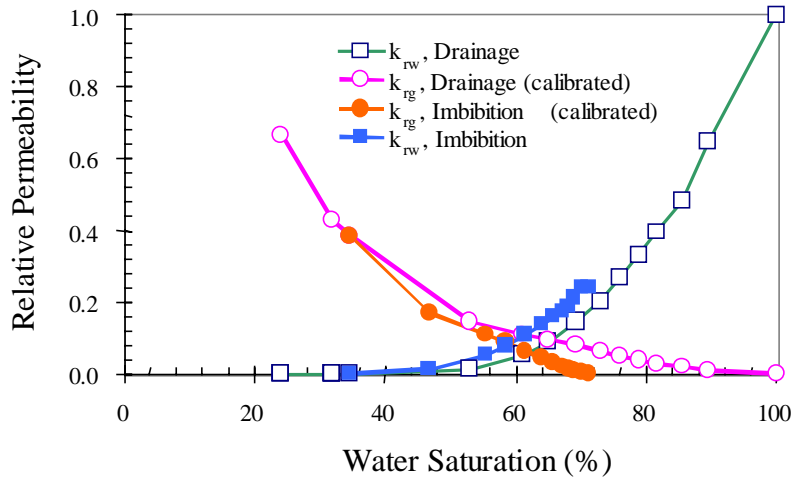


Figure 5.7: Imbibition and drainage gas-water relative permeabilities (with correction of gas slippage).

5.6 DISCUSSION

As a matter of experimental practicality, steam-water or gas-water relative permeabilities are usually measured at a low mean pressure. When the steam-water relative permeabilities are reported to the reservoir engineers, the corresponding experimental mean pressures may not be included within the report. It is known from the analysis reported here that gas relative permeabilities may change with the mean pressure. The reservoir pressure is generally much higher than the experimental pressure. So, if reservoir engineers apply the experimental data of relative permeabilities in reservoir calculations, significant error may occur. The solution to this problem is clear. The no-slip steam relative permeabilities independent of test pressure should be computed and reported to reservoir engineers together with the corresponding steam slip factors. Therefore, reservoir engineers can use Equations 5.5-5.7 to calculate the steam relative permeabilities at whatever pressures are required.

5.7 CONCLUSIONS

Based on the present work, the following conclusions may be drawn:

1. At certain conditions, gas slippage affects steam flow properties significantly; neglecting the steam slip effect in a steam-water two-phase flow may overestimate steam relative permeabilities and hence overestimate the productivity of geothermal wells.
2. It is necessary to measure the steam relative permeabilities at different mean pressures and then calculate the no-slip relative permeabilities using the method developed in this study.
3. The no-slip steam relative permeabilities are of importance in reservoir engineering, numerical simulation, and for applying the experimental results at the geothermal reservoir scale.
4. The effect of water saturation on gas slippage (slip factor and intrinsic effective gas permeability) is significant and a linear correlation between the gas slip factor and the effective intrinsic gas permeability at different water saturations is observed on a log-log plot.
5. An accurate method has been devised for measuring the water saturation in steady-state relative permeability tests for gas-water and two-phase flow.

5.8 FUTURE WORK

We will develop an apparatus for measuring the slip factor of steam and use the measured value of steam-slip factor to calculate the no-slip steam phase relative permeabilities. The effect of temperature on steam slip factor will be also investigated.

6. REFERENCES

Ambusso, W., Satik, C., Horne, R. (1996), "A Study of Relative Permeability for Steam-Water Flow in Porous Media," Proceedings of 21st Workshop on Geothermal Reservoir Engineering, Stanford University, Stanford, California.

Ambusso, W., Satik, C., and Horne, R.N.: "Determination of Relative Permeability for Steam-Water Flow in Porous Media," paper SPE 36682, presented at the 1996 Annual Technical Conference and Exhibition, Denver, Colorado, Oct. 6-9.

Counsil, J.R.: "Steam-Water Relative Permeability," Ph.D. Dissertation, Stanford University, May, 1979.

Guerrero, M., Satik, C., Finsterle, S., and Horne, R. (1998), "Inferring Relative Permeability From Dynamic Boiling Experiments," Proceedings of 23rd Workshop on Geothermal Reservoir Engineering, Stanford University, Stanford, California.

Handy, L.L.: "Determination of Effective Capillary Pressures for Porous Media from Imbibition Data," Petroleum Transactions AIME, Vol. 219, 1960, 75-80.

Herkelrath, W.N., Moench, A.F., and O'Neal II, C.F.: "Laboratory Investigations of Steam Flow in a Porous Medium," *Water Resources Research*, Vol. 19, No.4, (August 1983), 931-937.

Horne, R.N., Ramey, H.J. Jr., Shang, S., Correa, A., and Hornbrook, J.: "The Effects of Adsorption and Desorption on Production and Reinjection in Vapor-Dominated Geothermal fields," Proc. Of the World Geothermal Congress 1995, Florence, Italy, May, 1995, 1973-1977.

Horne, R. (1991), Notes on Geothermal Reservoir Engineering, Stanford University, Stanford, California.

Jones, F.O. and Owens, W.W.: "A Laboratory Study of Low-Permeability Gas Sands," *JPT* (September 1980), 1631-1640.

Klinkenberg, L.J.: "The Permeability of Porous Media to Liquids and Gases," *Drill. Prod. Prac.*, API (1941), 200-213.

Mahiya, G. and Horne, R. (1998), "Measurements of Steam-Water Relative Permeability," Stanford Geothermal Program Quarterly Report April-June 1998, Stanford University, Stanford, California.

Persoff, P. and Hulen, J.B.: "Hydrologic Characterization of Four Cores from the Geysers Coring Project," Proc. of 21rd Workshop on Geothermal Reservoir Engineering, Stanford, Calif., 1996.

Sampath, K.: "Factors Affecting Gas Slippage in Tight Sandstones of Cretaceous Age in the Uinta Basin," *JPT* (November 1982), 2715-2720.

Satik, C. (1997), "Experiments of Boiling in Porous Media," Proceedings of 22nd Workshop on Geothermal Reservoir Engineering, Stanford University, Stanford, California.

Satik, C. (1998), "A Measurement of Steam-Water Relative Permeability," Proceedings of 23rd Workshop on Geothermal Reservoir Engineering, Stanford University, Stanford, California.

Sta. Maria, R.B.S. and Pingol, A.: "Simulating the Effects of Adsorption and Capillary Forces in Geothermal Reservoirs," Proc. of 21st Workshop on Geothermal Reservoir Engineering, Stanford, Calif., 1996.

Schembre, J.M., Akin, S., Castanier, L.M., and Kovsky, A.R.: "Spontaneous Water Imbibition into Diatomite," paper SPE 46221, presented at the 1998 Western Region Meeting, Bakersfield, California, May 10-13.

Satik, C. and Horne, R.N.: "Measurement of Steam-Water Relative Permeability," Quarterly report for January – March 1998 Stanford Geothermal Program, DE-FG07-95ID13370.

Urmeneta, N.A., Fitzgerald, S., and Horne, R.N.: "The Role of Capillary Forces in the Natural State of Fractured Geothermal Reservoirs," Proc. of 23rd Workshop on Geothermal Reservoir Engineering, Stanford, Calif., 1998.

Wel, K.K., Morrow, N.R., and Brower, K.R.: "Effect of Fluid, Confining Pressure, and Temperature on Absolute Permeabilities of Low-Permeability Sandstones," *SPE Formation Evaluation* (August 1986), 413-423.